Article Identifier
DOI: 10.22032/dbt.58739
URN: urn:nbn:de:gbv:ilm1-2023isc-082:3

60th ILMENAU SCIENTIFIC COLLOQUIUM
Technische Universität Ilmenau, 4 – 8 September 2023
URN: urn:nbn:de:gbv:ilm1-2023isc:1

A LASER BEAM DEFLECTION SYSTEM FOR HEAT TREATMENTS IN LARGE SCALE ADDITIVE MANUFACTURING

Michel Layher[1,3], Jens Bliedtner[1], and René Theska[2]*

[1]Ernst-Abbe-Hochschule Jena, 07745 Jena, Germany
[2]Technische Universität Ilmenau, 98693 Ilmenau, Germany
[3]Carl Zeiss Jena GmbH, 07745 Jena, Germany
*michel.layher@zeiss.com

ABSTRACT

Large Scale Additive Manufacturing (LSAM) based on plastic raw material is known for high material output and thus, increased productivity. For an improvement of part properties LSAM is combined with a laser process. Depending on the deposition direction, the laser beam needs to be repositioned to reach the space between two adjacent and consecutively printed strands. Therefore, an optomechanical design is required that allows variable orientation of the laser beam. It consists of a combination of an elliptical, tube-like mirror with an additional, rotatable flat mirror in one of its focal axes. The deflected laser beam hits the second focal axis where the extruder nozzle is located. Thus, > 75% of the nozzle circumference is covered during a laser beam treatment. Both mirrors are individually designed custom-made parts. Its functional verification lays the foundation for an improved additive manufacturing process, which aims to homogenize the component structures to improve the mechanical properties of 3D-printed components.

Index Terms – Optomechanical Mirror Setup, Laser Beam Deflection System, Elliptical Tube-like Mirror, Large Scale Additive Manufacturing (LSAM), Hybrid Additive Manufacturing

1. INTRODUCTION AND BACKGROUND

Additive Manufacturing (AM) describes a wide area of technologies and processes for industrial applications. Especially, granule-based extrusion technologies such as Large Scale Additive Manufacturing (LSAM) enable high mass output and enhance the variety of materials used for strand deposition [1]. LSAM realizes parts by melting polymer granules through a heated extruder and the material deposition on a platform, according to a desired geometry. Within the last years knowledge about the process behaviour has been continuously extended [2-4]. Also, experimental setups have been evolved into automated manufacturing systems for industrial applications [5,6].

LSAM achieves part properties which are basically comparable to those of Fused-Filament-Fabrication (FFF). However, due to larger nozzle diameters (>3 mm) process related defects become even more obvious and occur bigger in shape [7]. This leads to a more orthotropic part behaviour and mechanical properties become strongly dependent on external loads.

In extrusion-based AM fracture resistance is primarily affected by inter- and intra-layer adhesion as well as the occurrence of voids and its size [8,9]. Investigations show that voids can be minimized by higher printing temperatures, although distortion and part deformation might occur as a negative side effect [8,10,11]. Especially in LSAM this effect is intensified since void size is increased with bead width [12]. Therefore, a suitable compromise between nozzle temperature and resulting structure is necessary. Furthermore, additional energy treatments are a considerable option to remelt deposited strands and solidify the parts.

In order to mitigate the mentioned characteristics, several laser beam heat treatment approaches have been developing for FFF during the last years, e.g. [13-15]. A new approach has been transferring this principle from FFF to LSAM. Laser radiation is directed onto deposited strands in order to reheat defined areas locally and increase interlayer as well as intra-layer bond [16]. Since polymers provide wavelength-dependent absorption properties [17] laser selection is also associated with the chosen materials as well as necessary additives. On the other hand, there are materials such as styrene-acrylonitrile-copolymer (SAN - TYRIL 790 - Trinseo) and poly(methyl methacrylate) (PMMA – Altuglas VSUVT) which provide perfect properties regarding a carbon dioxide laser (CO_2) beam treatment of unmodified raw material [18].

However, strand deposition direction is changed based on the part's geometry and the manufacturing routine, so the laser beam needs to be redirected as well. Several concepts of deflection systems were systematically developed, compared, and evaluated according to the

desired requirements. A preferred solution was found based on a combination of a fixed elliptical tube-like mirror and a rotating plane deflection mirror [19]. Thus, a mirror based, optomechanical system for multidirectional laser beam propagation is chosen. Such a setup appears to be very promising for part optimization [20] and describes a new approach in LSAM.

2. TECHNICAL DESIGN

The technical design of the laser beam deflection system is derived from the concretized technical principle and the shape synthesis [19]. The aim here is to transfer the partial results obtained into an overall solution and thus complete the design phase of the constructive design process.

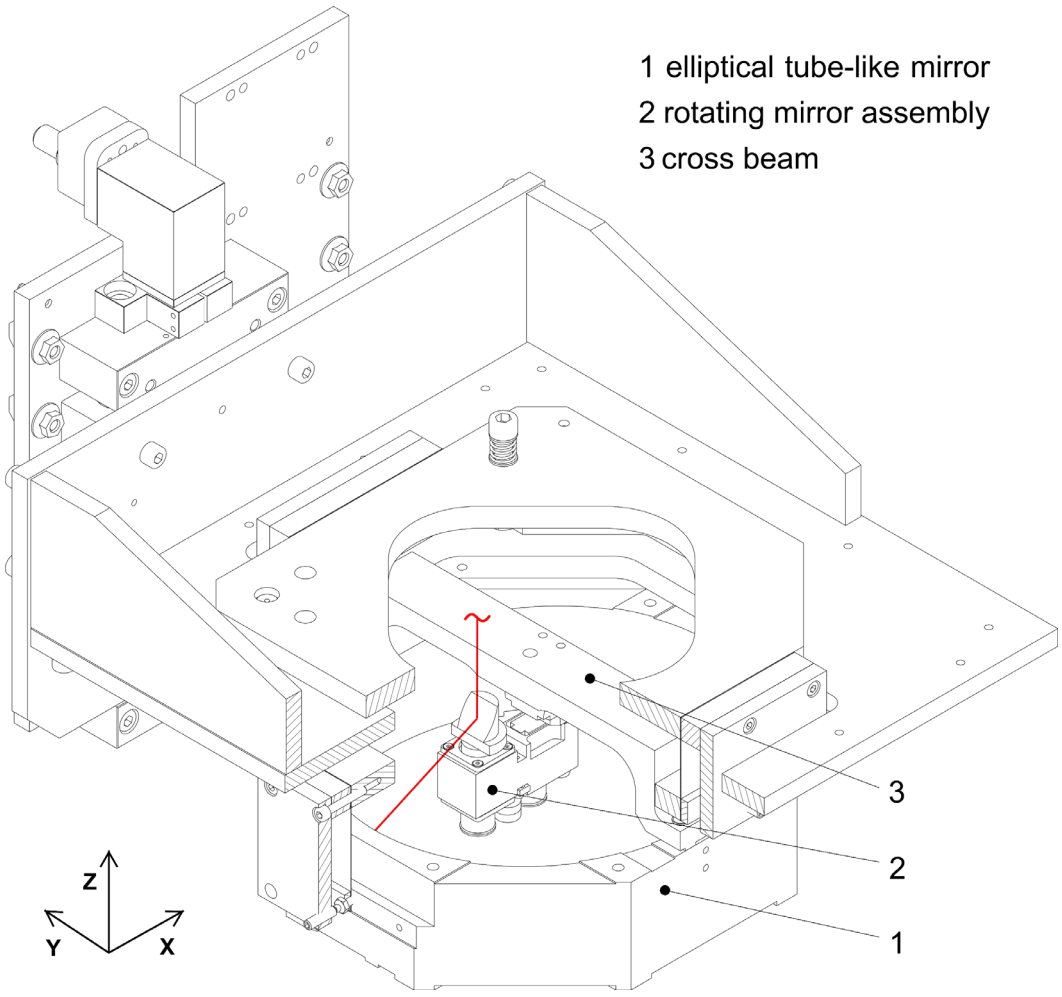

Figure 1: Laser beam deflection system in partial sectional view

The design of the laser beam deflection system is shown in Figure 1. For better clarity, other machine components including the extruder are not shown. According to the concretised

technical principle, the combination of the elliptical tube-like mirror (1) and rotating mirror assembly (2) as well as the implementation of the required adjustment points of the laser beam deflection system is carried out. By integrating the rotating mirror assembly within the elliptical tube-like mirror by means of a cross beam (3), a very compact design is made possible without impairing the deflection principle. The system-related shadowing during tempering is limited by the existing extruder diameter and thus reduced to the achievable minimum. Depending on the maximum laser beam diameter of $d_f = 7.5 \pm 0.5$ mm, the maximum usable swivel angle is $\alpha_{Rot} = \pm 157°$ and thus, approximately 75 % of the circumference at the extruder nozzle is covered. The elliptical tube-like mirror (M_2) and the corresponding rotating mirror (M_1) are individual custom-made products (cf. Figure 2).

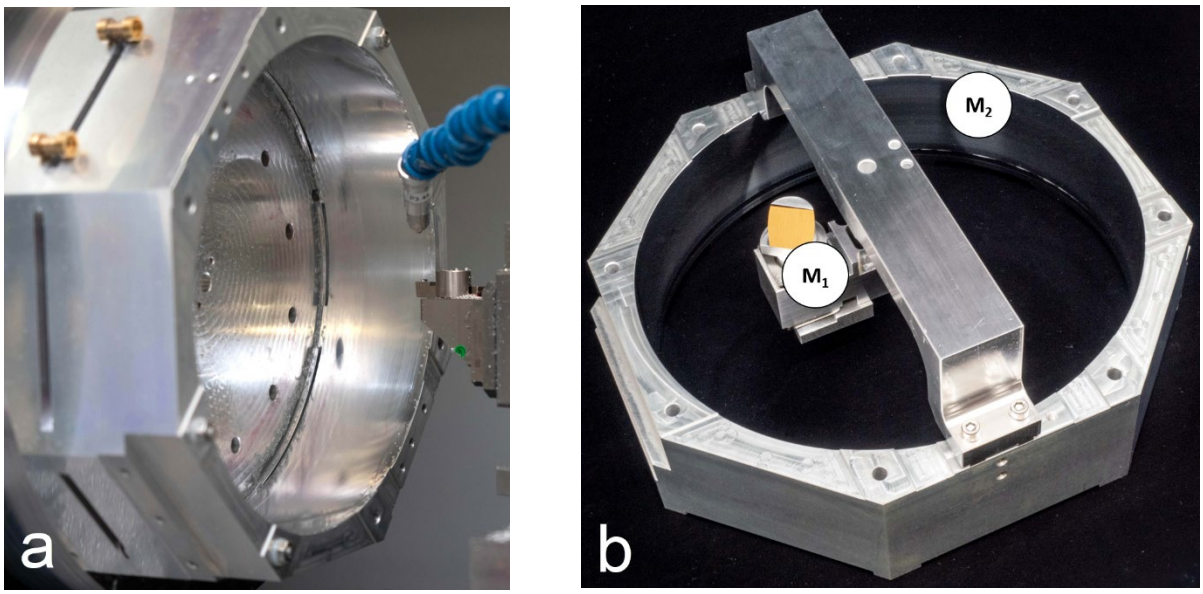

Figure 2: Ultraprecision turning (a) and pre-assembled mirror-system (b) [20]

The mirror surfaces are produced directly in a pre-machined mechanical carrier, based on a high-quality aluminum alloy by means of 5-axis diamond turning, thus there is no need for additional coating of these surfaces. In order to precisely coordinate the position of the individual components, the machining sequence is based on a defined flow chart. Elements of the overall system are pre-assembled between the individual production steps and machined according to the principle of joint production. By means of a 3D coordinate measuring machine, it is also possible to adjust the rotating mirror to the left-hand focal axis of the elliptical tube-like mirror. This means that the system can later be integrated into the machine structure as an independent module.

3. FUNCTIONAL VERIFICATION AND CHARACTERISATION OF THE LASER BEAM DEFLECTION SYSTEM

After setting up and adjusting the system, the functionality of the laser beam deflection system must be proven. To do this, it is first necessary to demonstrate the functional relationship between the angle of rotation to be controlled (α_{Rot}) and the temperature control angle (ω) at the effective zone (Figure 3).

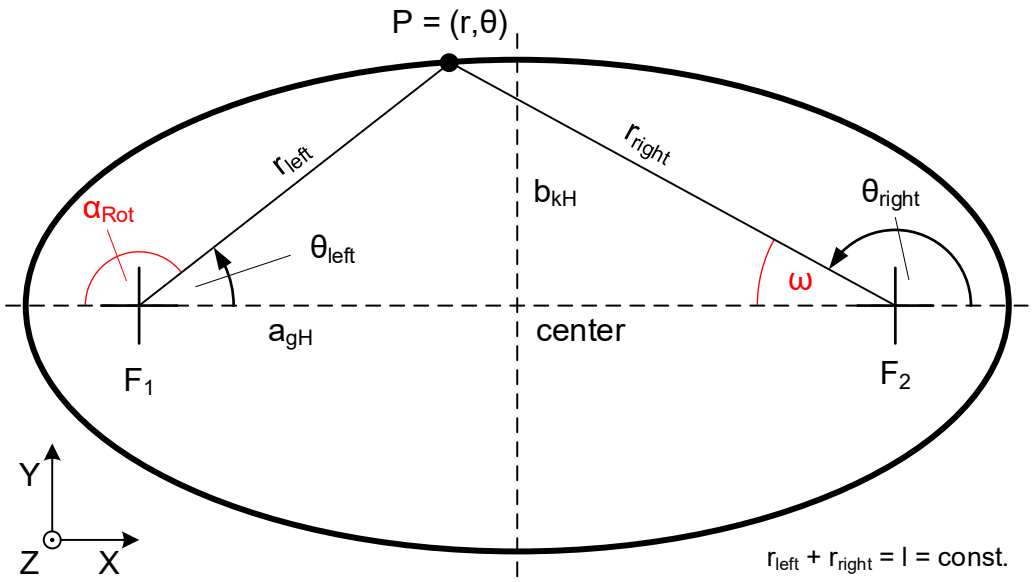

Figure 3: Ellipse relations in polar coordinates with pole in the focal point - principle in top-view

The description of the ellipse is done via polar coordinates with respect to the pole in the respective focal point F_1 or F_2 [21]. Thus, it follows:

$$r_{\mathrm{left}}(\theta_{\mathrm{left}}) = \frac{{b_{\mathrm{kH}}}^2}{a_{\mathrm{gH}}} \cdot \frac{1}{1 - \epsilon \cdot \cos\theta_{\mathrm{left}}} \tag{1}$$

and

$$r_{\mathrm{right}}(\theta_{\mathrm{right}}) = \frac{{b_{\mathrm{kH}}}^2}{a_{\mathrm{gH}}} \cdot \frac{1}{1 + \epsilon \cdot \cos\theta_{\mathrm{right}}}, \tag{2}$$

with the numerical eccentricity of the ellipse:

$$\epsilon = \frac{\sqrt{{a_{\mathrm{gH}}}^2 - {b_{\mathrm{kH}}}^2}}{a_{\mathrm{gH}}}, \quad (\epsilon > 1). \tag{3}$$

For ellipses, $l = r_{\mathrm{left}} + r_{\mathrm{right}}$, the relationship:

$$\omega(\alpha_{\mathrm{Rot}}) = 180° - arcCos\left[\frac{{b_{\mathrm{kH}}}^2 \cdot (a_{\mathrm{gH}} - f_{\mathrm{lE}} \cdot \cos(180° - \alpha_{\mathrm{Rot}}))}{\left(l \cdot (a_{\mathrm{gH}} - f_{\mathrm{lE}} \cdot \cos(180° - \alpha_{\mathrm{Rot}})) - {b_{\mathrm{kH}}}^2\right) \cdot f_{\mathrm{lE}}} - \frac{a_{\mathrm{gH}}}{f_{\mathrm{lE}}}\right] \tag{4}$$

is given under consideration of:

$$f_{\mathrm{lE}} = \sqrt{{a_{\mathrm{gH}}}^2 - {b_{\mathrm{kH}}}^2}\,. \tag{5}$$

a_{gH} major semi-axis of the ellipse

b_{kH} minor semi-axis of the ellipse

f_{lE} linear eccentricity of the ellipse

Formula (4) is used to determine the resulting tempering angle depending on the angular position of the rotating mirror. The mathematical relationship can now be integrated into a corresponding software (Arduino Integrated Development Environment) and linked to the associated control computer of the laser beam deflection system (Arduino Uno Rev3). This is also connected to the PLC of the axis system. A hall sensor picks up the original position of the rotating mirror. Via the output of an analogue voltage signal of the machine control (control computer of the axis system) to the control unit of the rotating mirror (control computer of the deflection system), the coupling of the machine feed vector with the direction of rotation of the mirror can take place, whereby the tracking of the laser radiation along the component path is realized. The rotating mirror has no mechanical stops and can therefore perform an endless rotation.

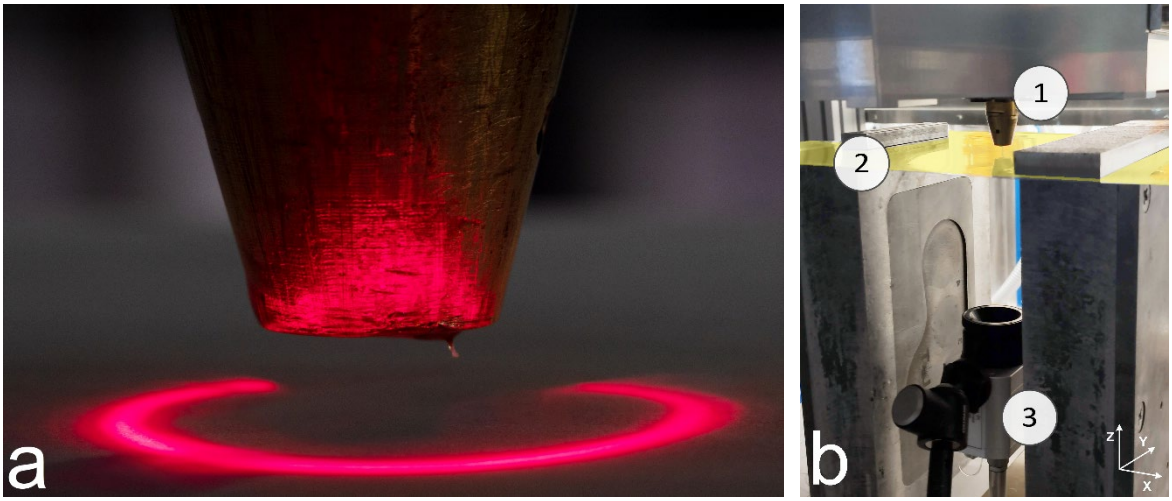

Figure 4: Testing of the functional principle (a) [20] and measurement setup for thermographic determination of the effective zone formation (b)

This makes it possible to map the available effective zone i.e., the maximum temperature range on the building platform with the help of the pilot laser (Figure 4, left), which is located inside the laser shutter. The result confirms in qualitative form the functionality of the principle of the preferred solution described in the principle synthesis [19].

In a further step, the qualitative determination of the effective zone formation within the working plane is carried out. The measurement setup is consisting of the elliptical tube-like mirror and the extruder nozzle (1), a plastic film (2) and a thermographic camera (3), cf. Figure 4b. The rotating mirror position is set to different angles. At a laser power of $P_L = 2$ W the laser beam is projected onto the plastic film (2) for $t = 0.2$ s and the resulting interaction is recorded by the thermographic camera from the underside.

This allows a comparison of the simulated interaction zone (Figure 5, upper row) with the thermographic measurement data (Figure 5, lower row), which proves the simulation results.

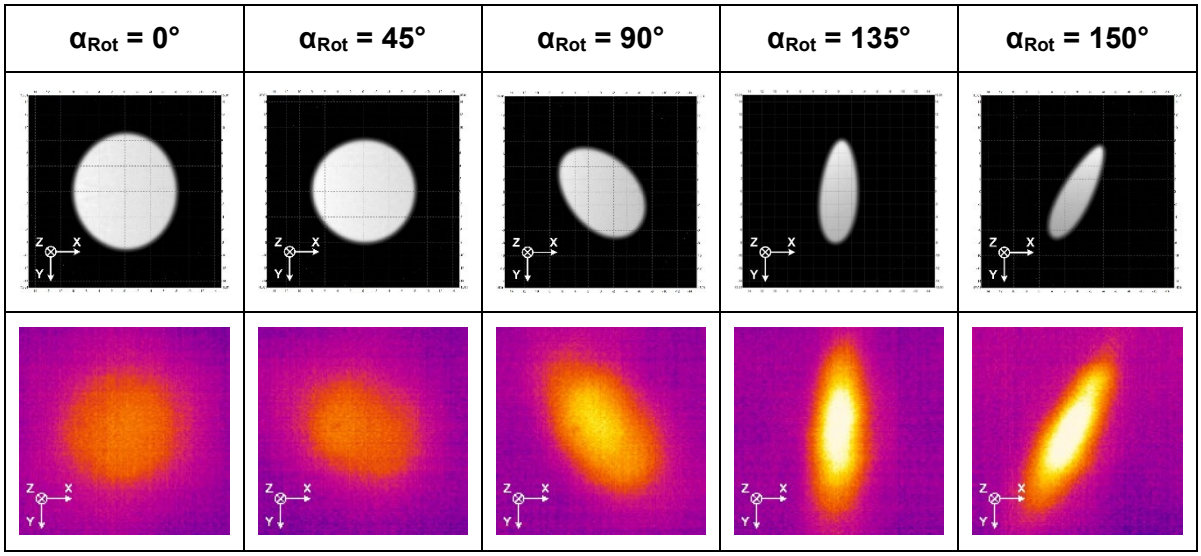

Figure 5: Qualitative comparison of the simulation (top) with the thermographic measurements (bottom)

Due to the slow reaction of the used laser system, no active control of the energy input can be performed in the combined process. On the other hand, it is necessary to deal with the occurring effect of different intensity profiles to avoid degradation of the polymer strands. However, in addition to tracking the laser beam along the machine's manufacturing path, a superimposed movement of the laser spot is possible, too. Using a specific amplitude ($\hat{u}$), the rotating mirror is dynamically pivoted within an angular range and therefore, the energy input is homogenized. Consequently, a gentle heat treatment of the polymer parts along different printing directions is achieved (cf. Figure 6a). This behaviour is also confirmed at the maximum amplitude of $\hat{u} = 150°$ (Figure 6b).

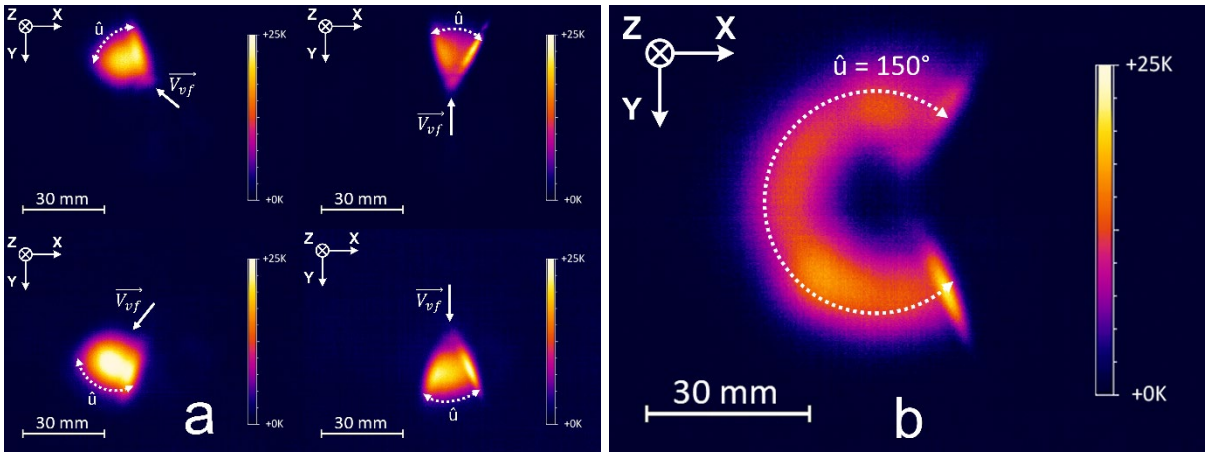

Figure 6: Representation of the homogenized energy input along different feed directions ($\overrightarrow{V_{vf}}$) with $\hat{u}$ = 20° (a) and maximum amplitude $\hat{u}$ = 150° (b)

In order to gain a quantitative description of the tempering process, power losses at the mirror system are investigated as well. The measurements are carried out using the power meter 1000W-BB-34 from Ophir. Laser output power is set to P_L = 30%, 50% and 70%. Within the angular limitation of the rotating mirror $\alpha_{Rot} = \pm$ 150° different measurement points are chosen, and the dynamic tempering is conducted using $\hat{u}$ = 10° and 20°.

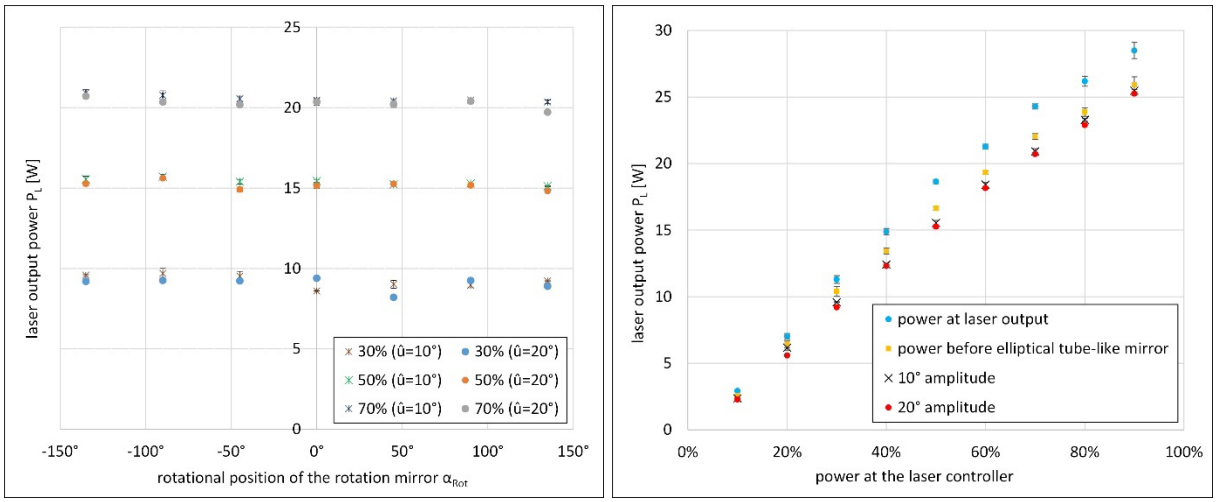

Figure 7: Display of the power measurement

It is found that the laser power remains constant within the entire measurement range and is neither influenced by the rotational position (α_{Rot}) nor the amplitude ($\hat{u}$) (Figure 7, left). At the same time, the results show that the elliptical tube-like mirror has a homogeneous reflectivity on its surface. Smaller deviations of the measuring points are due to fluctuations of the laser system.

In a second step, the energy loss due to beam guidance and reflection at mirror surfaces is detected. In doing so, the laser output power is measured directly at the laser output, after

passing through all beam guiding mirrors but before the elliptical tube-like mirror and in the interaction zone ($\hat{u}$ = 10°, 20°). As a result, it is found that the entire mirror setup leads to an average power loss of approximately 15 % (Figure 7, right). This must be considered in further investigations. On the other hand, different amplitudes do not show any influence on the measurements.

In the combined process of additive manufacturing and laser beam heat treatment, the heated field is converted into a heated line due to the movement of the axis system. Dependent on the size of the selected amplitude, there are differences in the temperature distribution (Figure 8).

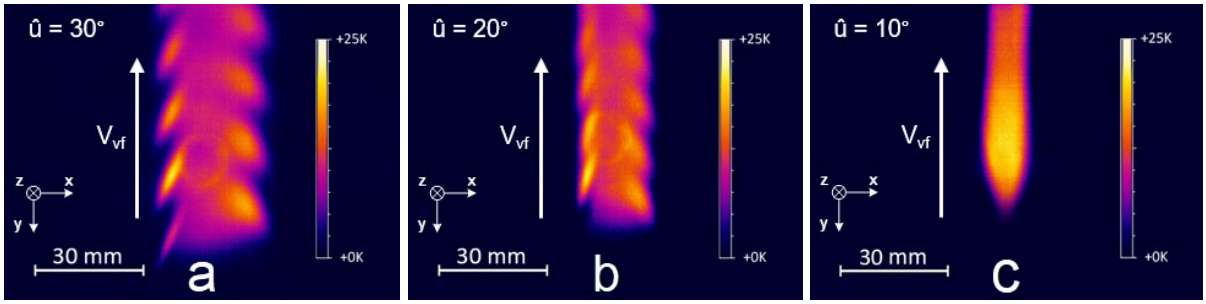

Figure 8: Representation of the emerging temperature profile by superimposing the vector of the machine feed ($\overrightarrow{V_{vf}}$) with the mirror swiveling at $\hat{u}$ = 30° (a), $\hat{u}$ = 20° (b) and $\hat{u}$ = 10° (c) [20]

Here a fundamental correlation between the machine feed and the dynamic heat treatment process can be seen. A greater amplitude ($\hat{u}$) leads to a more irregular temperature distribution. This results in temperature peaks, related to the reversal points of the mirror swiveling. The preliminary test shows that there is a homogeneous temperature distribution at $\hat{u}$ = 10°.

Based on the described experiments as well as the characterizations carried out, the functionality of the laser beam deflection system was proven and can therefore be used without restrictions for further investigations.

4. LOCALISED HEAT TREATMENT USING THE LASER BEAM DEFLECTION SYSTEM

The combination of large scale additive manufacturing with the localized heat treatment laser beam deflection system allows two steps within one process. Not only the top surface of the strands is hit by the laser energy but also the lateral remelting of the strands is achieved. So, improved component properties can be expected as a result.

A particular advantage of the laser beam deflection system is the dynamic tempering, which allows quasi-simultaneous heating of horizontal and lateral areas at extrudate strands. To determine the process window, the material heating (ΔT) on the respective underlying strand (Spot A) and adjacent strand (Spot B) is observed, shown in Figure 9a.

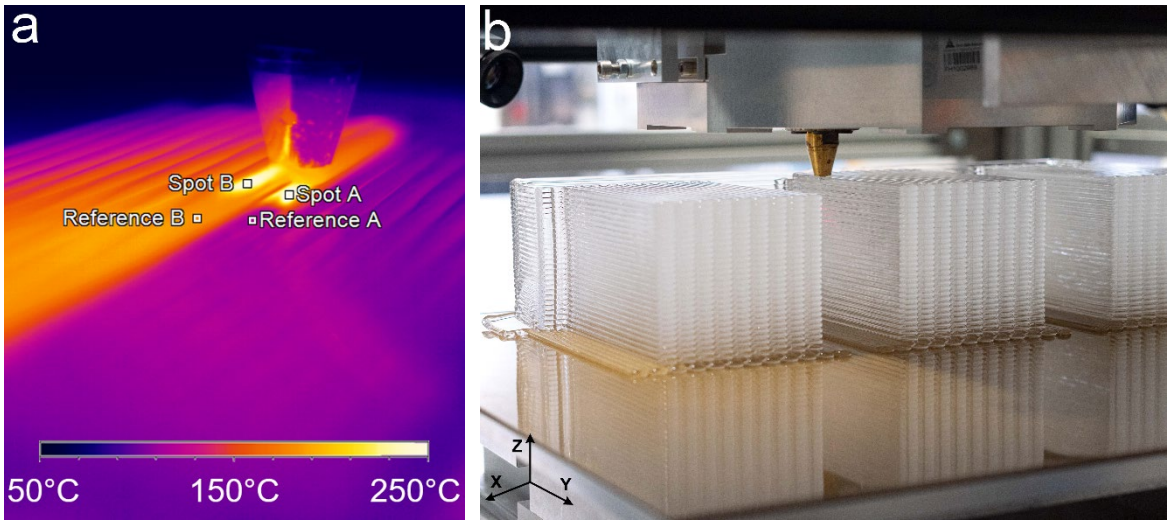

Figure 9: Representation of the measuring fields on the underlying and adjacent material strand during dynamic tempering (a) [20] and component production (b)

Depending on the laser power (P_L) and different rotating mirror amplitudes ($\hat{u}$ = 10°, 15°, 20°), the process windows for PMMA and SAN can be generated (Figure 10). The limiting condition here is the decomposition of the plastics, which manifests itself in the form of smoke formation. The results show that a lower rotating mirror amplitude leads to greater heating at the same laser power. Thus, $\hat{u}$ = 10° can be confirmed as the ideal parameter for the dynamic tempering of both plastics, since the tempered field has a very good homogeneity. This leads to a better utilization of the laser power.

As a result, all the process parameters required for the combined process with laser beam deflection system are now available. The lateral melting of the strands allows the track overlap to be increased to a maximum of q = 0.5 mm.

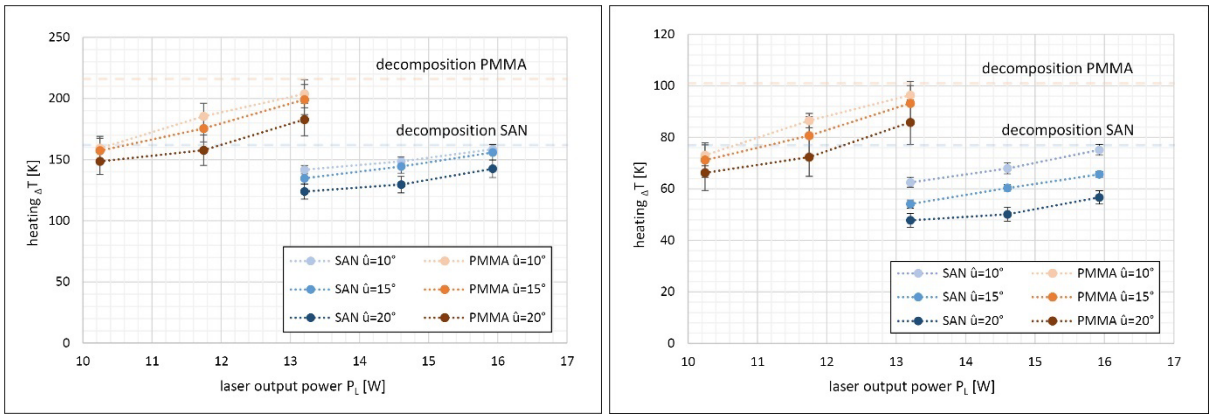

Figure 10: Representation of the material heating as a function of laser output power and rotation angle amplitude for PMMA and SAN for the material strand below (left) and the material strand next to it (right)

For the visual analysis of the internal component structure three cuboid components are produced simultaneously from PMMA and SAN (cf. Figure 9b).

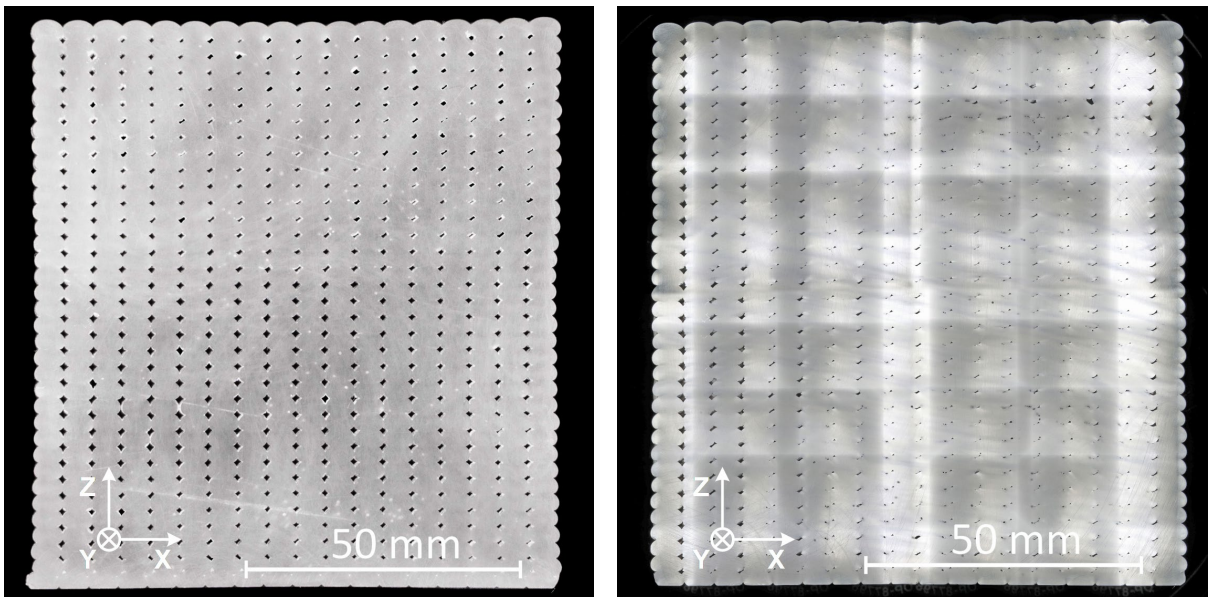

Figure 11: Cross-section of a PMMA test specimen before (left) and after (right) the laser beam heat treatment

By means of cross-sectional analysis (Figure 11) it is possible to evaluate the resulting component structure. The analysis shows a significant reduction of the cavity size while maintaining the shape of the component. Within the component, voids remain with an areal proportion of 1.2 % for PMMA and 3.4 % for SAN. This corresponds to a reduction of 82 % for PMMA and 76 % for SAN compared to the conventional large scale additive manufacturing process. PMMA performs better than SAN in terms of void reduction. In addition, it is

confirmed that the density of the components increases in the production direction (along the X-axis).

5. RESULTS

After the implementation and alignment of the system, a good agreement of the performance with the simulation results could be demonstrated. In addition to the beam guidance along the printing path, a superimposed oscillating movement enables a homogenization of the irradiation. Thus, simultaneous heat treatment of the underlying and adjacent strands becomes possible. Based on the results, it can be proven that the process combination with a laser beam deflection system leads to a clear approximation to isotropic component structures, in particular with regard to the lateral void formation. The utilization of the opto-mechanical system represents a new approach in enhanced LSAM processes as well as an extension of the state of the art. It is already proven that a significant improvement of LSAM parts can be achieved [20]. Further investigations will not only focus on other amorphous plastics but also semicrystalline polymers as well as composites of glass, metals, and ceramics.

REFERENCES

[1] Justino Netto, Joaquim Manoel; Idogava, Henrique Takashi; Frezzatto Santos, Luiz Eduardo; Silveira, Zilda de Castro; Romio, Pedro; Alves, Jorge Lino (2021): Screw-assisted 3D printing with granulated materials: a systematic review. In: Int J Adv Manuf Technol, S. 1–17. DOI: 10.1007/s00170-021-07365-z.

[2] Schmidt, Leander; Schricker, Klaus; Bergmann, Jean Pierre; Hussenöder, Felix; Eiber, Mathias (2018): Characterization of a granulate-based strand deposition process in the FLM-method for definition of material-dependent process strategies. In: Rapid Prototyping Journal 25 (1), S. 104–116. DOI: 10.1108/RPJ-09-2017-0186.

[3] Schilling, M.; Bliedtner, J. (2020): Konzeptionelle Entwicklung und Bau einer hochproduktiven Fertigungsanlage zur generativen Herstellung großvolumiger Bauteile aus wahlfreien Kunststoffen. HP3D: Verlag Ernst-Abbe-Hochschule Jena.

[4] Layher, Michel; Eckhardt, Lukas; Hopf, Andreas; Bliedtner, Jens (2021): Development of a Process Model for Bead Deposition Rates and Cooling Behavior of Large Scale Additive Manufacturing Parts. In: Industrializing Additive Manufacturing - AMPA, S. 223–240. DOI: 10.1007/978-3-030-54334-1_16.

[5] Cincinnati Incorporated (2015): BAAM (Big Area Additive Manufacturing). Online https://3dprintingindustry.com/news/research-institutions-collaborate-local-motors-big-area-additive-manufacturing-composite-materials-111446/, last accessed: 03.12.2021.

[6] Thermwood (2017): LSAM (Large Scale Additive Manufacturing). online http://thermwood.com/lsam/brochures/lsam_2017_brochure/index.html#?page=8, last accessed: 03.12.2021.

[7] Duty, Chad E.; Kunc, Vlastimil; Compton, Brett; Post, Brian; Erdman, Donald; Smith, Rachel et al. (2017): Structure and mechanical behavior of Big Area Additive Manufacturing (BAAM) materials. In: Rapid Prototyping Journal 23 (1), S. 181–189. DOI: 10.1108/RPJ-12-2015-0183.

[8] Aliheidari, Nahal; Christ, Josef; Tripuraneni, Rajasekhar; Nadimpalli, Siva; Ameli, Amir (2018): Interlayer adhesion and fracture resistance of polymers printed through melt extrusion additive manufacturing process. In: Materials & Design 156, S. 351–361. DOI: 10.1016/j.matdes.2018.07.001.

[9] Papon, Easir Arafat; Haque, Anwarul; Mulani, Sameer B. (2019): Process optimization and stochastic modeling of void contents and mechanical properties in additively manufactured composites. In: Composites Part B: Engineering 177, S. 107325. DOI: 10.1016/j.compositesb.2019.107325.

[10] Turner, Brian N.; Gold, Scott A. (2015): A review of melt extrusion additive manufacturing processes: II. Materials, dimensional accuracy, and surface roughness. In: Rapid Prototyping Journal 21 (3), S. 250–261. DOI: 10.1108/RPJ-02-2013-0017.

[11] Kuznetsov, Vladimir E.; Solonin, Alexey N.; Tavitov, Azamat G.; Urzhumtsev, Oleg D.; Vakulik, Anna H. (2018): Increasing of Strength of FDM (FFF) 3D Printed Parts by Influencing on Temperature-Related Parameters of the Process. DOI: 10.20944/preprints201803.0102.v2.

[12] Eiliat, Hasti; Urbanic, Jill (2018): Visualizing, analyzing, and managing voids in the material extrusion process. In: Int J Adv Manuf Technol 96 (9-12), S. 4095–4109. DOI: 10.1007/s00170-018-1820-5.

[13] Ravi, Abinesh Kurapatti; Deshpande, Anagh; Hsu, Keng H. (2016): An in-process laser localized pre-deposition heating approach to inter-layer bond strengthening in extrusion based polymer additive manufacturing. In: Journal of Manufacturing Processes 24, S. 179–185. DOI: 10.1016/j.jmapro.2016.08.007.

[14] Luo, Meng; Tian, Xiaoyong; Zhu, Weijun; Li, Dichen (2018): Controllable interlayer shear strength and crystallinity of PEEK components by laser-assisted material extrusion. In: J. Mater. Res. 33 (11), S. 1632–1641. DOI: 10.1557/jmr.2018.131.

[15] Kühn, Cornelius; Niese, Bernd; Witt, Gerd (2019): Verbesserung der mechanischen Eigenschaften im FLM-Verfahren durch lokale Laservorerwärmung und Endlosfaserverstärkung. In: Proceedings of the 16th Rapid.Tech Conference Erfurt, Germany, 25 – 27 June 2019, S. 258–273.

[16] Layher, Michel; Eckhardt, Lukas; Linke, Daniel; Hopf, Andreas; Bliedtner, Jens (2023): Laser beam heat treatment in large-scale additive manufacturing. In: Prog Addit Manuf. DOI: 10.1007/s40964-023-00415-w.

[17] Bliedtner, Jens; Müller, Hartmut; Barz, Andrea (2013): Lasermaterialbearbeitung. Grundlagen - Verfahren - Anwendungen - Beispiele. München: Carl Hanser Fachbuchverlag. Online verfügbar unter http://www.hanser-elibrary.com/action/showBook?doi=10.3139/9783446429291.

[18] Layher, Michel; Hopf, Andreas; Eckhardt, Lukas; Bliedtner, Jens (2019): Laser Beam Polishing of Polymers. In: PhotonicsViews 16 (3), S. 83–87. DOI: 10.1002/phvs.201900025.

[19] Layher, Michel; Bliedtner, Jens; Theska, René (2021): Development of a laser beam deflection system for hybrid large scale additive manufacturing. euspen's 21st International Conference & Exhibition, Copenhagen, DK, June 2021. In: Proceedings of the 21st International Conference of the European Society for Precision Engineering and Nanotechnology, S. 75–78.

[20] Layher, Michel; Bliedtner, Jens; Theska, René (2022): Hybrid additive manufacturing. In: PhotonicsViews 19 (5), S. 47–51. DOI: 10.1002/phvs.202200041.

[21] Papula, Lothar (2017): Mathematische Formelsammlung. Wiesbaden: Springer Fachmedien Wiesbaden.

ACKNOWLEDGEMENT

This project is supported by the Federal Ministry for Economic Affairs and Climate Action (BMWK) on the basis of a decision by the German Bundestag. (Funding number: KK5091602SK0). We would also like to thank our partners Granula Deutschland for supporting us in material sourcing and Spaceoptix for the continuous support during the development and manufacturing of the mirror system.

CONTACTS

Michel Layher email: michel.layher@zeiss.com
ORCID: https://orcid.org/0000-0002-5433-7720

Prof. Dr.-Ing. Jens Bliedtner email: jens.bliedtner@eah-jena.de
ORCID: https://orcid.org/0000-0002-0824-1509

Prof. Dr.-Ing. René Theska email: rene.theska@tu-ilmnenau.de
ORCID: https://orcid.org/0000-0003-0589-8270

